Implementation of drift velocities and currents in SOLEDGE2D-EIRENE

Hugo Bufferand, C Baudoin, J Bucalossi, G Ciraolo, Julien Denis, Nicolas Fedorczak, D Galassi, Philippe Ghendrih, R Leybros, Y Marandet, et al.

Implementation of drift velocities and currents in SOLEDGE2D-EIRENE

H. Bufferand[a], C. Baudoin[a], J. Bucalossi[a], G. Ciraolo[a], J. Denis[a], N. Fedorczak[a], D. Galassi[c], Ph. Ghendrih[a], R. Leybros[c], Y. Marandet[b], N. Mellet[b], J. Morales[d], N. Nace[a], E. Serre[c], P. Tamain[a], M. Valentinuzzi[a]

a CEA, IRFM, 13108 St Paul-Lez-Durance, France.

b PIIM - CNRS Aix-Marseille Université - 13397 Marseille, France

c M2P2 - CNRS Aix-Marseille Université - 13451 Marseille, France

d Swiss Plasma Center - EPFL - Lausanne, Switzerland

Abstract

In order to improve cross-field transport description, drifts and currents have been implemented in SOLEDGE2D-EIRENE. The derivation of an equation for the electric potential is recalled. The resolution of current equation is tested in a simple slab case. WEST divertor simulations in forward-B and reverse-B fields are also discussed. A significant increase of ExB shear is observed in the forward-B configuration that could explain a favorable L-H transition in this case.

1. Introduction

By their ability to gather multiple physics from plasma transport, neutral physics to plasma wall interaction, transport codes remain key tools to interpret experiments and extrapolate observations to future machine like ITER or DEMO. In that perspective, a dedicated effort has been paid in the last few years to develop the code SOLEDGE2D-EIRENE [1] focusing on treating the plasma wall interaction with all the plasma facing components including the first wall. This contribution describes recent progress to include the effect of transport due to drifts velocities. Besides, solving drifts velocities also requires revisiting perpendicular momentum balance in order to derive an equation for the electric potential. Inclusion of drifts in transport codes [2, 3, 4, 5] is often reported as being challenging and we find appropriate giving motivations and justifications for the model we use to solve electric potential (currents) equation.

So far, the perpendicular tranport in SOLEDGE2D-EIRENE has only consisted in an effective diffusion accounting for a coarse-grained description of the turbulent transport. More precisely, considering for instance continuity equation, density and velocity can be decomposed into an averaged and a fluctuating component, the average being taken over scales and times much longer than typical turbulence scales. Following this decomposition, density can be expressed as $n = \langle n \rangle + \tilde{n}$ with $\tilde{n}$ the fluctuating part. Averaging continuity equation yields

$$\partial_t \langle n \rangle + \vec{\nabla} \cdot (\langle n \rangle \langle \vec{v} \rangle + \langle \tilde{n} \tilde{v} \rangle) = \langle S_n \rangle. \tag{1}$$

The flux due to fluctuations is expressed as a diffusive flux: $\langle \tilde{n} \tilde{v} \rangle = -D \vec{\nabla}_\perp \langle n \rangle$. Remains an averaged flux due to advection by averaged parallel and perpendicular velocity. In addition to the parallel and effective turbulent transport, a proper description of plasma transport with a code like SOLEDGE2D-EIRENE thus requires a proper description of the cross-field transport due to averaged perpendicular velocities also called averaged drift velocities. Next section describes the derivation of these velocities and their implementation in SOLEDGE2D.

2. Drifts and currents in SOLEDGE2D-EIRENE

2.1. Derivation of cross-B velocities

The derivation of drifts and currents relies mostly on perpendicular momentum balance. For all species in the plasma (electrons, main ions, impurities), the fluid velocity evolves according to equation 2.

$$\frac{\partial}{\partial t}(mn\vec{v}) + \vec{\nabla} \cdot (mn\vec{v} \otimes \vec{v}) = -\vec{\nabla} p - \vec{\nabla} \cdot \bar{\bar{\Pi}} + qn\left(\vec{E} + \vec{v} \times \vec{B}\right) + \vec{S}_v \tag{2}$$

The perpendicular velocity is expressed by multiplying equation 2 by $\vec{B}\times$ giving,

$$\begin{aligned} \vec{v}_\perp &= \frac{\vec{b}}{n\omega_c} \times \left[\frac{\partial}{\partial t}(n\vec{v}) + \vec{\nabla} \cdot (n\vec{v} \otimes \vec{v})\right] \\ &+ \frac{\vec{B} \times (\vec{\nabla} p + \vec{\nabla} \cdot \bar{\bar{\Pi}})}{qnB^2} + \frac{\vec{E} \times \vec{B}}{B^2} - \frac{\vec{B} \times \vec{S}_v}{qnB^2} \end{aligned} \tag{3}$$

Following the drift ordering, one writes $\vec{v}_\perp = \vec{v}_\perp^{(0)} + \varepsilon \vec{v}_\perp^{(1)} + \dots$ where $\varepsilon = \tau_c/\tau_f$ is a small parameter where τ_f is the typical evolution time of fluid moments $1/\tau_f = d/dt$ and $\tau_c = 1/\omega_c$ is the cyclotronic time. The stress tensor $\bar{\bar{\Pi}}$ can be expressed as $\bar{\bar{\Pi}} = \bar{\bar{\Pi}}^{FLR} + \bar{\bar{\Pi}}^{vis}$ where $\bar{\bar{\Pi}}^{FLR}$ is the collisionless gyroviscous stress-tensor and $\bar{\bar{\Pi}}^{vis}$ gathers

collisional effects [6]. In this contribution, we retain only the parallel part of the viscous stress tensor giving:

$$\bar{\bar{\Pi}}^{vis} = \bar{\bar{\Pi}}_{\parallel} = \pi_{\parallel}\left(\vec{b}\otimes\vec{b} - \frac{1}{3}\bar{\bar{I}}\right) \tag{4}$$

where $\pi_{\parallel} = p_{\parallel} - p_{\perp}$. According to Braginski's closure [7, 6], $\pi_{\parallel} = -3\eta_0(\nabla_{\parallel}v_{\parallel} - \vec{\kappa}\cdot\vec{v} - \vec{\nabla}\cdot\vec{v}/3)$ with the magnetic field curvature $\vec{\kappa} = \vec{b}\cdot\vec{\nabla}\vec{b} = -\vec{b}\times(\vec{\nabla}\times\vec{b})$ [1]. The divergence of this tensor is given by

$$\begin{aligned}\vec{\nabla}\cdot\bar{\bar{\Pi}}_{\parallel} &= -\frac{1}{3}\vec{\nabla}\pi_{\parallel} + (\vec{\nabla}\cdot\pi_{\parallel}\vec{b})\vec{b} + \pi_{\parallel}\vec{b}\cdot\vec{\nabla}\vec{b} \\ &= -\frac{1}{3}\vec{\nabla}\pi_{\parallel} + (\vec{\nabla}\cdot\pi_{\parallel}\vec{b})\vec{b} + \pi_{\parallel}\vec{\kappa}\end{aligned} \tag{5}$$

The perpendicular velocity can be developped as

$$\begin{aligned}\vec{v}_{\perp} &= \frac{\vec{E}\times\vec{B}}{B^2} + \frac{\vec{B}\times\vec{\nabla}p}{qnB^2} + \frac{\vec{B}\times\vec{\nabla}\cdot\bar{\bar{\Pi}}_{\parallel}}{qnB^2} \\ &\quad + \frac{m\vec{B}\times\vec{\nabla}\cdot(nv_{\parallel}^2\vec{b}\otimes\vec{b})}{qnB^2} - \frac{\vec{B}\times\vec{S}_v}{qnB^2} + \varepsilon\vec{v}_{\perp}^{(1')} \\ &= \frac{\vec{E}\times\vec{B}}{B^2} + \frac{\vec{B}\times\vec{\nabla}(p - 1/3\pi_{\parallel})}{qnB^2} \\ &\quad + \frac{mnv_{\parallel}^2 + \pi_{\parallel}}{qnB^2}\vec{B}\times\vec{\kappa} - \frac{\vec{B}\times\vec{S}_v}{qnB^2} + \varepsilon\vec{v}_{\perp}^{(1')}\end{aligned} \tag{6}$$

where we have defined a first order in ε velocity

$$\begin{aligned}\varepsilon\vec{v}_{\perp}^{(1')} &= \frac{\vec{b}}{n\omega_c}\times\left[\frac{\partial}{\partial t}(n\vec{v}_{\perp}) + \vec{\nabla}\cdot(n\vec{v}_{\perp}\otimes\vec{v})\right. \\ &\quad \left. + \vec{\nabla}\cdot\left(nv_{\parallel}\vec{b}\otimes\vec{v}_{\perp}\right) + \vec{\nabla}\cdot\bar{\bar{\Pi}}^{FLR}\right]\end{aligned} \tag{7}$$

It is assumed here that the drift velocity associated with the divergence of the gyro-viscous stress tensor is a first order velocity in the drift ordering. This point will be discussed in the following paragraph concerning momentum transport by drifts. Given that $p = (p_{\parallel} + 2p_{\perp})/3$, one recovers in Equation 6 the expression given by Chankin in [2]:

$$\begin{aligned}\vec{v}_{\perp} &= \frac{\vec{E}\times\vec{B}}{B^2} + \frac{\vec{S}_v\times\vec{B}}{qnB^2} + \frac{\vec{B}\times\vec{\nabla}p_{\perp}}{qnB^2} \\ &\quad + \frac{\left(mnv_{\parallel}^2 + p_{\parallel} - p_{\perp}\right)}{qnB^3}\vec{B}\times\vec{B}\cdot\vec{\nabla}\left(\frac{\vec{B}}{B}\right)\end{aligned} \tag{8}$$

The perpendicular velocity is decomposed into the "E cross B" velocity $\vec{v}_E = \vec{E}\times\vec{B}/B^2$, the diamagnetic velocity $\vec{v}_d = (\vec{B}\times\vec{\nabla}p_{\perp})/(qnB^2)$, the curvature drift velocity $\vec{v}_c = (mnv_{\parallel}^2 + p_{\parallel} - p_{\perp})/(qnB^2)\vec{B}\times\vec{\kappa}$ and a drift due to collisions with other species $\vec{v}_{col} = \vec{S}_v\times\vec{B}/(qnB^2)$. It is not clear whether $\vec{v}_c$ is 0^{th}-order or 1^{st}-order velocity in the drift ordering since it is a curvature term and thus relatively small. Comparing with diamagnetic drift gives $v_c/v_d \approx M^2\rho_i/R = M^2\rho^{\star}$. In the drift ordering, it is assumed that $\varepsilon \sim \rho^{\star 2}$, a small Mach number is often assumed also. The curvature drift is thus considered as a 1^{st}-order term in the drift ordering here. The 0^{th}-order velocity is finally given by the sum of "E cross B", diamagnetic and collision drift velocities.

$$\vec{v}_{\perp}^{(0)} = \frac{\vec{E}\times\vec{B}}{B^2} + \frac{\vec{B}\times\vec{\nabla}p_{\perp}}{qnB^2} + \frac{\vec{S}_v\times\vec{B}}{qnB^2} \tag{9}$$

Remains at first order:

$$\varepsilon\vec{v}_{\perp}^{(1)} = \varepsilon\vec{v}_{\perp}^{(1')} + \frac{mnv_{\parallel}^2 + \pi_{\parallel}}{qnB^2}\vec{B}\times\vec{\kappa} \tag{10}$$

Using vector identity $\vec{A}\times\vec{\nabla}f = f\vec{\nabla}\times\vec{A} - \vec{\nabla}\times(f\vec{A})$, the diamagnetic flux can be rewritten extracting the divergence free contribution:

$$\begin{aligned}n\vec{v}_d &= \frac{\vec{B}\times\vec{\nabla}p_{\perp}}{qB^2} \\ &= \vec{\nabla}\times\vec{K} + \frac{2p_{\perp}\vec{B}\times\vec{\nabla}B}{qB^3} + \frac{p_{\perp}}{qB^2}\vec{\nabla}\times\vec{B} \\ &= \vec{\nabla}\times\vec{K} + n\tilde{v}_d\end{aligned} \tag{11}$$

where $\vec{K} = -p_{\perp}\vec{B}/(qB^2)$ and $\vec{\nabla}\times\vec{K}$ is the so-called magnetization flux. The velocity $\tilde{v}_d$ associated with the motion of guiding centers is defined by:

$$\tilde{v}_d = \frac{2T_{\perp}\vec{B}\times\vec{\nabla}B}{qB^3} + \frac{T_{\perp}}{qB^2}\vec{\nabla}\times\vec{B} \tag{12}$$

the second term in the RHS being negligible in the low-β limit. One has by construction $\vec{\nabla}\cdot(n\vec{v}_d) = \vec{\nabla}\cdot(n\tilde{v}_d)$. More generally, one has $\vec{\nabla}\cdot(n\vec{v}) = \vec{\nabla}\cdot(n\tilde{v})$ where $\tilde{v} = \vec{v} - \vec{v}_d + \tilde{v}_d$.

The first order velocity $\vec{v}_{\perp}^{(1)}$ can be found by reinjecting the expression for $\vec{v}_{\perp}^{(0)}$ in Equation 2. Before going any further, let us express the divergence of the gyro-viscous stress tensor. Many expression for this term can be found in the litterature following various approximations [8, 9, 10, 6]. We retain here the expression given by Chang in [10]:

$$\vec{\nabla}\cdot\bar{\bar{\Pi}}^{FLR} = -nm\vec{v}_d\cdot\vec{\nabla}\vec{v} + (\vec{\nabla}_{\perp} + 2\vec{b}\nabla_{\parallel})\chi + \frac{p_{\perp}}{\omega_c}(\vec{b}\times\vec{\nabla})\nabla_{\parallel}v_{\parallel} \tag{13}$$

where $\chi = -(p_{\perp}/\omega_c)\vec{b}\cdot(\vec{\nabla}_{\perp}\times\vec{v})$. In a more compact way we write $\vec{\nabla}\cdot\bar{\bar{\Pi}}^{FLR} = -nm\vec{v}_d\cdot\vec{\nabla}\vec{v} + \vec{\nabla}\cdot\bar{\bar{\Pi}}^{FLR*}$ where the first term will play a role in the so-called diamagnetic cancellation. The second term gathers other finite Larmor radius effects that we neglect latter on in SOLEDGE. Reporting in Equation 2 and developping momentum advection gives:

$$\begin{aligned}\partial_t(mn\vec{v}) + \left[\vec{\nabla}\cdot(mn\vec{v})\right]\vec{v} + mn\vec{v}\cdot\vec{\nabla}\vec{v} = \\ -\vec{\nabla}p + mn\vec{v}_d\cdot\vec{\nabla}\vec{v} - \vec{\nabla}\cdot\left(\bar{\bar{\Pi}}^{vis} + \bar{\bar{\Pi}}^{FLR*}\right) \\ + qn\left(\vec{E} + \vec{v}\times\vec{B}\right) + \vec{S}_v\end{aligned} \tag{14}$$

[1] Note that $\vec{\kappa}\cdot\vec{b} = 0$. Besides the magnetic curvature $\vec{\kappa}$ can be developped as $\vec{\kappa} = (\vec{\nabla}_{\perp}B)/B + \mu_0(\vec{\nabla}_{\perp}p)/B^2$. The second term vanishes in the low-β limit.

The second term in the LHS can be rewritten using $\vec{\nabla}\cdot(n\vec{v}) = \vec{\nabla}\cdot(n\tilde{v})$. The third term in he LHS can be combined with the second term in the RHS (diamagnetic cancellation). Remains a term link with advection by $\tilde{v}_d$ that can be gathered with the remaining FLR terms. Equation 14 can thus be rewritten as:

$$\begin{aligned}\partial_t(mn\vec{v}) + \left[\vec{\nabla}\cdot(mn\tilde{v})\right]\vec{v} + mn\tilde{v}\cdot\vec{\nabla}\vec{v} = \\ -\vec{\nabla}p + mn\tilde{v}_d\cdot\vec{\nabla}\vec{v} - \vec{\nabla}\cdot\left(\bar{\bar{\Pi}}^{vis} + \bar{\bar{\Pi}}^{FLR*}\right) \\ +qn\left(\vec{E} + \vec{v}\times\vec{B}\right) + \vec{S}_v \qquad (15)\end{aligned}$$

or finally

$$\begin{aligned}\partial_t(mn\vec{v}) + \vec{\nabla}\cdot(mn\tilde{v}\otimes\vec{v}) &= -\vec{\nabla}p - \vec{\nabla}\cdot\left(\bar{\bar{\Pi}}^{vis} + \bar{\bar{\Pi}}^{FLR\dagger}\right) \\ &\quad +qn\left(\vec{E} + \vec{v}\times\vec{B}\right) + \vec{S}_v \qquad (16)\end{aligned}$$

with

$$\begin{aligned}\vec{\nabla}\cdot\bar{\bar{\Pi}}^{FLR\dagger} &= -mn\tilde{v}_d\cdot\vec{\nabla}\vec{v} + \vec{\nabla}\cdot\bar{\bar{\Pi}}^{FLR*} \qquad (17)\\ &= -\left(\frac{2p_\perp}{\omega_c B}\vec{b}\times\vec{\nabla}B + \frac{p_\perp}{\omega_c B}\vec{\nabla}\times\vec{B}\right)\cdot\vec{\nabla}\vec{v} \\ &\quad +(\vec{\nabla}_\perp + 2\vec{b}\nabla_\parallel)\chi + \frac{p_\perp}{\omega_c}(\vec{b}\times\vec{\nabla})\nabla_\parallel v_\parallel\end{aligned}$$

This term is neglected in the following. Taking the scalar product of Equation 16 with $\vec{b}$ gives parallel momentum equation:

$$\partial_t(mnv_\parallel) + \vec{\nabla}\cdot(mn\tilde{v}v_\parallel) = -\nabla_\parallel p_\parallel - \pi_\parallel\vec{\nabla}\cdot\vec{b} + qnE_\parallel + \vec{S}_{v_\parallel} \qquad (18)$$

Taking cross-product of Equation 16 with $\vec{b}/(n\omega_c)$, we recover first order drift velocities of course and we can now express the 1st order velocity we left over at the beginning of the section, also called polarization drift $\vec{v}_{pola} = \varepsilon\vec{v}_\perp^{(1')}$:

$$\begin{aligned}\vec{v}_{pola} &= \frac{\vec{b}}{n\omega_c}\times\left[\frac{\partial}{\partial t}\left(n\vec{v}^{(0)}\right) + \vec{\nabla}\cdot\left(n\vec{v}^{(0)}\otimes\vec{v}^{(0)}\right)\right. \\ &\quad \left.-\vec{\nabla}\cdot\left(nv_\parallel^2\vec{b}\otimes\vec{b}\right)\right] + \frac{\vec{B}\times\vec{\nabla}\cdot\bar{\bar{\Pi}}^{FLR}}{qnB^2} \\ &= \frac{\vec{b}}{n\omega_c}\times\left[\frac{\partial}{\partial t}\left(n\vec{v}^{(0)}\right) + \vec{\nabla}\cdot\left(n\tilde{v}^{(0)}\otimes\vec{v}^{(0)}\right)\right. \\ &\quad \left.-\vec{\nabla}\cdot\left(nv_\parallel^2\vec{b}\otimes\vec{b}\right)\right] \qquad (19)\end{aligned}$$

Denoting $\vec{\omega} = -(\vec{b}/\omega_c)\times(n\vec{v}^{(0)})$, the particle flux associated to this velocity can be developped according to Equation 20:

$$\begin{aligned}n\vec{v}_{pola} &= \frac{\vec{b}}{\omega_c}\times\left[\frac{\partial}{\partial t}\left(n\vec{v}^{(0)}\right) + \vec{\nabla}\cdot\left(n\tilde{v}_\perp^{(0)}\otimes\vec{v}^{(0)}\right) + \vec{\nabla}\cdot\left(nv_\parallel\vec{b}\otimes\vec{v}_\perp^{(0)}\right)\right] \\ &= -\partial_t\vec{\omega} - \left(\vec{\nabla}\cdot\tilde{v}_\perp^{(0)}\right)\vec{\omega} + \frac{\vec{b}}{\omega_c}\times\left[\tilde{v}_\perp^{(0)}\cdot\vec{\nabla}(n\vec{v}^{(0)})\right] - \left(\vec{\nabla}\cdot v_\parallel\vec{b}\right)\vec{\omega} + \frac{\vec{b}}{\omega_c}\times\left[v_\parallel\vec{b}\cdot\vec{\nabla}(n\vec{v}_\perp^{(0)})\right] \\ &= -\partial_t\vec{\omega} - \left(\vec{\nabla}\cdot\tilde{v}^{(0)}\right)\vec{\omega} + \frac{\vec{b}}{\omega_c}\times\left[\tilde{v}^{(0)}\cdot\vec{\nabla}(n\vec{v}_\perp^{(0)})\right] + \frac{\vec{b}}{\omega_c}\times\left[\tilde{v}_\perp^{(0)}\cdot\vec{\nabla}(nv_\parallel\vec{b})\right] \\ &= -\partial_t\vec{\omega} - \left(\vec{\nabla}\cdot\tilde{v}^{(0)}\right)\vec{\omega} + \frac{\vec{b}}{\omega_c}\times\left[\tilde{v}^{(0)}\cdot\vec{\nabla}(n\vec{v}_\perp^{(0)})\right] + nv_\parallel\frac{\vec{b}}{\omega_c}\times\left[\tilde{v}_\perp^{(0)}\cdot\vec{\nabla}\vec{b}\right] \qquad (20)\end{aligned}$$

Using vectorial identity $\vec{A}\times(\vec{B}\cdot\vec{\nabla}\vec{C}) = \vec{B}\cdot\vec{\nabla}(\vec{A}\times\vec{C}) + \vec{C}\times(\vec{B}\cdot\vec{\nabla}\vec{A})$, the expression for polarization flux can further be simplified to

$$\begin{aligned}n\vec{v}_{pola} &= -\partial_t\vec{\omega} - \left(\vec{\nabla}\cdot\tilde{v}^{(0)}\right)\vec{\omega} - \tilde{v}^{(0)}\cdot\vec{\nabla}\vec{\omega} \\ &\quad +n\vec{v}_\perp^{(0)}\times\left[\tilde{v}^{(0)}\cdot\vec{\nabla}\left(\frac{\vec{b}}{\omega_c}\right)\right] + nv_\parallel\frac{\vec{b}}{\omega_c}\times\left[\tilde{v}_\perp^{(0)}\cdot\vec{\nabla}\vec{b}\right] \\ n\vec{v}_{pola} &= -\partial_t\vec{\omega} - \vec{\nabla}\cdot\left(\tilde{v}^{(0)}\otimes\vec{\omega}\right) \qquad (21) \\ &\quad +n\vec{v}_\perp^{(0)}\times\left[\tilde{v}^{(0)}\cdot\vec{\nabla}\left(\frac{\vec{b}}{\omega_c}\right)\right] + nv_\parallel\frac{\vec{b}}{\omega_c}\times\left[\tilde{v}_\perp^{(0)}\cdot\vec{\nabla}\vec{b}\right]\end{aligned}$$

In SOLEDGE2D, we neglect so far the two last curvature terms in the RHS of Equation 21 and finally obtain a compact expression for the polarization flux:

$$n\vec{v}_{pola} = -\partial_t\vec{\omega} - \vec{\nabla}\cdot\left(\tilde{v}^{(0)}\otimes\vec{\omega}\right) \qquad (22)$$

To be more precise, a thorough treatment of curvature terms should be done including those already dropped from the divergence of the gyroviscous tensor. This is beyond the scope of this contribution. Following Equation 6 for $\vec{v}_\perp^{(0)}$, $\vec{\omega}$ can be expressed as:

$$\begin{aligned}\vec{\omega} &= -\frac{\vec{b}}{\omega_c}\times\left(\frac{n\vec{B}\times\vec{\nabla}_\perp\phi}{B^2} + \frac{\vec{B}\times\vec{\nabla}_\perp(p - 1/3\pi_\parallel)}{qB^2} - \frac{\vec{B}\times\vec{S}_v}{qB^2}\right) \\ \vec{\omega} &= \frac{m}{qB^2}\left(n\vec{\nabla}_\perp\phi + \frac{1}{q}\vec{\nabla}_\perp\left(p - \frac{\pi_\parallel}{3}\right)\right) - \frac{m}{q^2B^2}\vec{S}_{v\perp} \qquad (23)\end{aligned}$$

2.2. Plasma current equation

Electric potential is determined from charge balance. The evolution of the charge is obtained summing continuity equations for all the species:

$$\frac{\partial}{\partial t}\left(\sum_\alpha q_\alpha n_\alpha\right) + \vec{\nabla}\cdot\left(\sum_\alpha q_\alpha n_\alpha\vec{v}_\alpha\right) = 0 \qquad (24)$$

According to quasineutrality, the first term vanishes giving $\vec{\nabla}\cdot\vec{j}=0$ where the current can be decomposed as:

- The parallel current $j_\parallel = \sum_\alpha q_\alpha n_\alpha v_{\parallel,\alpha}$
- The diamagnetic current $\vec{j_d} = \sum_\alpha q_\alpha n_\alpha \vec{v}_{d,\alpha}$
- The curvature current $\vec{j_c} = \sum_\alpha q_\alpha n_\alpha \vec{v}_{c,\alpha}$
- The collisonal current $\vec{j}_{col} = \sum_\alpha q_\alpha n_\alpha \vec{v}_{col,\alpha}$
- The polarization current $\vec{j}_{pola} = \sum_{\alpha\neq e} q_\alpha n_\alpha \vec{v}_{pola,\alpha}$

Reporting Equation 20 in the polarization current expression yields:

$$\vec{j}_{pola} = -\partial_t \vec{\omega}_s - \sum_{\alpha\neq e} q_\alpha \vec{\nabla}\cdot\left(\tilde{v}_\alpha^{(0)}\otimes\vec{\omega}_\alpha\right) \tag{25}$$

where the vector $\vec{\omega}_s$ is expressed as

$$\vec{\omega}_s = \sum_{\alpha\neq e} q_\alpha \vec{\omega}_\alpha \tag{26}$$

The vorticity Ω is defined by $\Omega = \vec{\nabla}\cdot\vec{\omega}_s$. The current equation $\vec{\nabla}\cdot\vec{j}=0$ can thus be rewritten as a transport equation of vorticity:

$$\partial_t\Omega + \vec{\nabla}\cdot\vec{F}_\Omega = \vec{\nabla}\cdot\left(j_\parallel\vec{b} + \vec{j_d} + \vec{j_c} + \vec{j}_{col}\right) \tag{27}$$

where the flux of vorticity $\vec{F}_\Omega$ is defined from equation 25:

$$\vec{F}_\Omega = \sum_{\alpha\neq e} q_\alpha \vec{\nabla}\cdot(\tilde{v}_\alpha\otimes\vec{\omega}_\alpha) \tag{28}$$

The parallel current is provided by the generalized Ohm law

$$j_\parallel = -\sigma_\parallel\left(\nabla_\parallel\phi - \frac{\nabla_\parallel p_e}{n_e e} - \frac{0.71}{e}\nabla_\parallel T_e\right) \tag{29}$$

where we use the simplified expression for parallel conductivity given in [11], valid for trace impurities in hydrogen plasma:

$$\sigma_\parallel = \eta_\parallel^{-1} = \left(Z_{eff}\times 0.51\frac{m_e}{n_e e^2\tau_e}\right)^{-1} \tag{30}$$

The boundary conditions for the electric potential at sheath entrance is given expressing net current on the wall:

$$j_\parallel^{wall} = e\left(\sum_\alpha Z_\alpha\Gamma_{\alpha,\parallel}\right)\exp\left(\Lambda - \frac{\phi_{se}-\phi_{wall}}{T_e}\right) \tag{31}$$

with

$$\Lambda = \log\left(\frac{1}{n_e}\sqrt{\frac{2\pi m_e}{T_e}}\sum_\alpha Z_\alpha\Gamma_{\alpha,\parallel}\right) \tag{32}$$

On any other boundary surface in the simulation domain such as the last flux surface simulated in the core plasma or any tangential wall, currents are forced to zero. In that manner, the only currents allowed to leave or enter the simulation domain are controled by sheath properties expressed in Equation 31.

2.3. Application to transport codes - turbulent closure

The vorticity evolution described by Equation 27 that we use to determine electric potential is valid at all spatial scales larger than Larmor radius and for time scales much greater than ion cyclotronic time. In transport codes, this equation is averaged over turbulent time scales and the turbulent fluctuations and subsequent transport are not directly resolved. A closure describing turbulent transport must be used. We propose here to introduce a diffusive closure to describe perpendicular currents due to turbulence. The final vorticity equation solved in SOLEDGE is finally

$$\partial_t\Omega + \vec{\nabla}\cdot\vec{F}_\Omega = \vec{\nabla}\cdot\left(j_\parallel\vec{b} + \vec{j_d} + \vec{j_c} + \vec{j}_{col}\right) + \vec{\nabla}\cdot\left(\zeta\vec{\nabla}_\perp\Omega\right) \tag{33}$$

where ζ is a turbulent vorticity diffusivity. The associated perpendicular current is $\vec{j}_{closure} = \zeta\vec{\nabla}_\perp\Omega$. All quantities in the above equation are averaged over turbulence time and are assumed axisymmetric. The effect of this "anomalous" current is mainly to stabilize electric potential evolution in the close field line regions where the integral of perpendicular current across flux surfaces must be zero.

3. Coupling with transport equations and implementation in SOLEDGE2D

3.1. Numerical implementation

The vorticity Equation 33 is solved directly as an equation on the electric potential ϕ. The vorticity Ω is expressed by a perpendicular Laplacian of the potential whereas the divergence of the parallel current exhibits the parallel Laplacian. The vorticity equation is thus a 2D strongly anistropic Laplace problem. It is made inversible as long as boundary conditions do not degenerate to Neumann boundary conditions. The boundary condition on the wall actually takes the form of a Robin boundary condition which makes the problem inversible. The vorticity equation discretization can be schematically written as:

$$(\tilde{\Delta}_\perp + \sigma_\parallel\tilde{\Delta}_\parallel)\phi_{i,j}^{t+dt} = \tilde{\Delta}_\perp\phi_{i,j}^t - \mathcal{A}(\phi_{i,j}^t) + RHS_{i,j} \tag{34}$$

where $\tilde{\Delta}_\perp$ denotes an inhomogeneous perpendicular Laplacian (including inhomogeneous space metric and density), $\tilde{\Delta}_\parallel$ denotes an inhomogeneous parallel Laplacian (including inhomogeneous metric and inhomogeneous parallel conductivity), $\mathcal{A}$ denotes divergence of F_Ω evaluated explicitely and RHS denotes all the other terms not depending on the electric potential. A direct inversion of the Laplacian operator is perfomed with the sparse matrix solver PASTIX [12]. The computation time dedicated to the inversion remains acceptable due to the small system size (about 10^4 degrees of freedom).

3.2. Coupling with transport equations

Once the potential is solved, drifts velocities are computed and added to transport equations. Table 1 sums up

	Without drifts	With drifts
Ions	$v_{\parallel,i}\vec{b} - D\frac{\vec{\nabla}_\perp n}{n}$	$v_{\parallel,i}\vec{b} - D\frac{\vec{\nabla}_\perp n}{n} + \vec{v}_E + \vec{v}_d^{\,i} + \vec{v}_c^{\,i} + \vec{v}_{col}^{\,i} + \vec{v}_{pola}$
Electrons	$v_{\parallel,i}\vec{b} - D\frac{\vec{\nabla}_\perp n}{n}$	$v_{\parallel,i}\vec{b} - D\frac{\vec{\nabla}_\perp n}{n} + \vec{v}_E + \vec{v}_d^{\,e} + \vec{v}_{col}^{\,e} - \frac{j_\parallel}{ne}\vec{b}$

Table 1: Summary of velocity definitions with and without drifts for ions and electrons.

definition of flow velocities with and without drifts (for a singly charged ion plasma for simplicity).

Boundary conditions are adapted on the wall to force the total plasma flux to escape with sound speed according to Bohm-Chodura boundary condition:

$$\begin{aligned} \|\tilde{v}\cdot\vec{n}_{wall}\| &= \left\|(v_{\parallel,i}\vec{b} + \vec{v}_E + \tilde{v}_d^{\,i} + \vec{v}_c + \vec{v}_{col}^{\,i})\cdot\vec{n}_{wall}\right\| \\ \|\tilde{v}\cdot\vec{n}_{wall}\| &\geq c_s\left\|\vec{b}\cdot\vec{n}_{wall}\right\| \end{aligned} \tag{35}$$

where $\vec{n}_{wall}$ is a unit vector orthogonal to the wall surface.

4. Tests in different configurations

4.1. Test of parallel boundary conditions in the SOL

Tests are performed in a simplified slab SOL configuration with open field lines only. The purpose is to test the resolution of the parallel current as well as the implementation of boundary conditions for the parallel current. One solves only $\vec{\nabla}\cdot(j_\parallel\vec{b}) = 0$ with the boundary condition given by Equation 31. The response of the plasma to wall polarization is tested by changing one target potential from -1000V to 1000V while the other target potential is set to the ground, see Figure 1. Perpendicular drifts velocity are not considered in transport equations. Figure 1 describes simulation results obtained with the left wall electric potential set to $200V$ while the right wall is grounded. A net parallel current is observed flowing from the left to the right. This current is higher in the hot region where the parallel resistivity is lower. In this simulation, electron temperature parallel gradients are small due to high enough parallel heat conductivity. Electric conductivity being also high, the effect of the biasing is small on ion balance and one keeps rather symmetric profiles for n_i (and thus n_e) and $\Gamma_i = n_i v_{\parallel,i}$. The electric potential follows $\log(n)$ and is also almost symmetric – not exactly symetric since a small parallel gradient is required to drive the parallel current. The effect of the biasing consists in modifying electron parallel velocity to create the parallel current. With a plasma temperature about $100eV$, when the wall is polarized to $200V$, most of the electrons flow toward the high voltage target while the electron flux on the grounded one is drastically reduced. In this situation, the current on the wall is close to the saturation current. The current dependence with the wall potential can be estimated considering that in this case, the potential gradients in the plasma are small compared with $\Delta\phi_{wall}$. The current on the left wall is given by

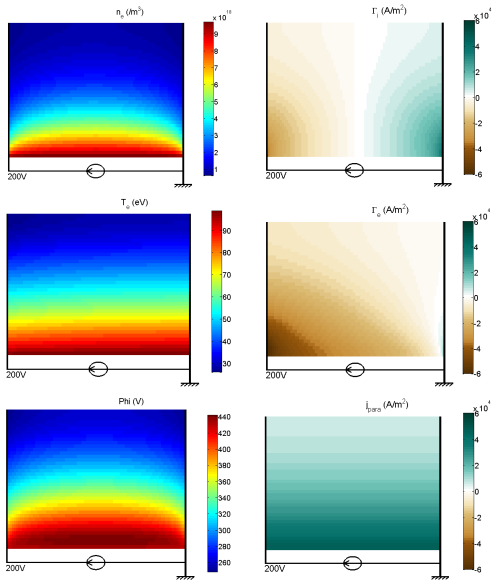

Figure 1: Simulation results for a simple slab scrape-off layer case. The left wall is polarized to 200V while the right wall is grounded.

$$j_L = e\Gamma_{i,L}\exp\left(\Lambda - \frac{\phi_L - \phi_{wall}}{T_e}\right) \tag{36}$$

and the current on the right wall is given by

$$j_R = e\Gamma_{i,R}\exp\left(\Lambda - \frac{\phi_R}{T_e}\right) \tag{37}$$

with $\phi_L \approx \phi_R$ and $\Gamma_{i,L} \approx -\Gamma_{i,R} = -j_{sat}/e$, one finds the I-V characteristic equation by solving $j_L = j_R = j$:

$$j = j_{sat}\left(1 - \frac{2}{1+\exp\left(-\phi_{wall}/T_e\right)}\right). \tag{38}$$

Figure 2 shows a comparison between SOLEDGE results and the above estimation for the I-V characteristic at the SOL entrance where the temperature is the highest. The two are in good agreement since in this case, the high electric conductivity hypothesis applies.

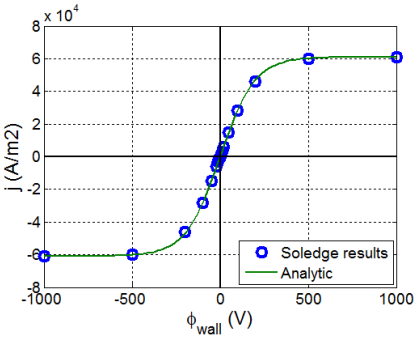

Figure 2: I-V characteristic of the slab SOL simulated in SOLEDGE (dots). Comparison with analytical estimation given by Equation 38.

4.2. Divertor flow pattern in complex geometry

To go further, a first application to the WEST divertor geometry has been achieved solving drifts and current taking into account the realistic magnetic and wall geometry of the machine. A low power ($P_{SOL} = 2MW$) L-mode discharge is considered. The electron density at the separatrix is $n_{e,sep} \approx 2 \cdot 10^{19} m^{-3}$ and $T_{e,sep} \approx 60eV$. Figure 3 shows electric potential profile in the low field side mid-plane for a forward-B configuration and a reverse-B configuration. A significantly higher shear of the radial electric field is found at the separatrix in the forward-B configuration in comparison with the reverse-B case which is alleged to make L-H transition more favorable in the forward-B case [13].

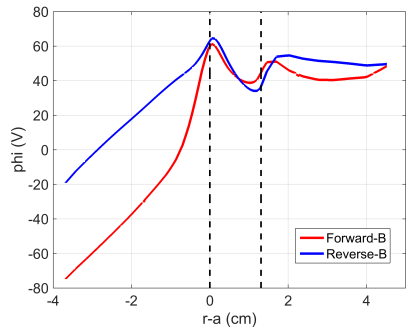

Figure 3: Radial profile of electric potential in a WEST configuration in Forward-B and Reverse-B configuration.

Figure 4 shows the "E cross B" velocity field in WEST divertor for the forward and reverse B configuration. A typical clockwise structure [3] can be observed in the forward B configuration with a flow circulating from the LFS to the HFS in the private flux region. The radial component of the "E cross B" drift flows from the LFS to the HFS. In the reverse B configuration, the stucture is reversed as expected. The highest shear of the "E cross B" velocity in the forward-B configuration is also visible.

5. Conclusion and perspectives

In order to improve the description of cross-field transport in SOLEDGE2D-EIRENE, drifts and currents have been implemented and successfully tested in a realistic WEST configuration up to the first wall. Further comparison with experiments must now be carried out to validate simulation results and confirm if the effect of mean-field drift velocities is well recovered by the code.

Acknowledgements

This work was granted access to the HPC resources of Aix-Marseille Université financed by the project Equip@Meso (ANR-10-EQPX-29-01) of the program "Investissements d'Avenir" supervised by the Agence Nationale pour la Recherche. This project has received funding from the European Union's Horizon 2020 research and innovation programme under grant agreement number 633053. The views and opinions expressed herein do not necessarily reflect those of the European Commision.

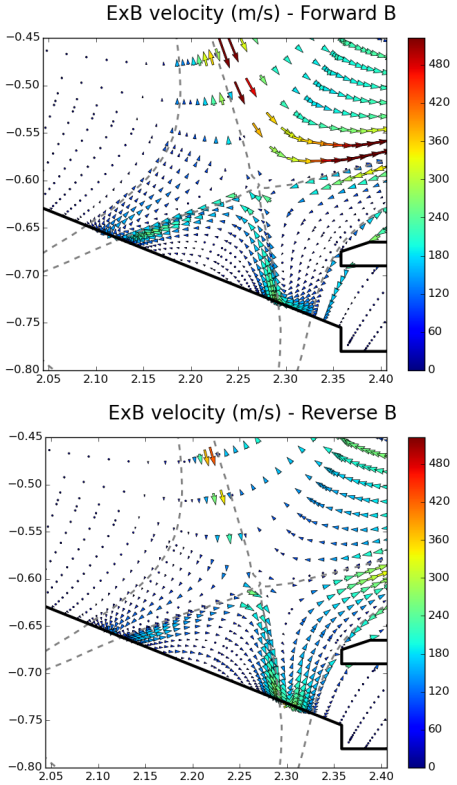

Figure 4: ExB velocity field in Forward and Reverse B configuration.

References

[1] H. Bufferand, G. Ciraolo, Y. Marandet, J. Bucalossi, P. Ghendrih, J. Gunn, N. Mellet, P. Tamain, R. Leybros, N. Fedorczak, F. Schwander, and E. Serre, "Numerical modelling for divertor design of the west device with a focus on plasma-wall interactions," *Nuclear Fusion*, vol. 55, p. 053025, 2015.

[2] A. V. Chankin, "Classical drifts in the tokamak sol and divertor: models and experiment," *J. Nuclear Materials*, vol. 241-243, pp. 199–213, 1997.

[3] T. Rognlien, G. Porter, and D. Ryutov, "Influence of e and drift terms in 2-d edge/sol transport simulations," *J. Nuclear Materials*, vol. 266-269, pp. 654–659, 1998.

[4] R. Pitts and *et al.*, "Edge and divertor physics ith reversed toroidal field in jet," *J. Nuclear Materials*, vol. 337-339, pp. 146–153, 2005.

[5] R. Schneider, X. Bonnin, K. Borrass, D. Coster, H. Kastelewicz, D. Reiter, V. Rozhansky, and B. Braams, "Plasma edge physics with b2-eirene," *Contrib. Plasma Phys.*, vol. 46, pp. 3–191, 2006.

[6] A. Zeiler, "Tokamak edge turbulence," Tech. Rep. 5/88, Max-Planck-Institut für Plasmaphysik, 1999.

[7] S. I. Braginskii, "Transport processes in a plasma," *Rev. of Plasma Phys.*, vol. 1, pp. 205–311, 1965.

[8] A. I. Smolyakov, "Gyroviscous forces in a collisionless plasma with temperature gradients," *Can. J. Phys.*, vol. 76, pp. 321–331, 1998.

[9] C. T. Hsu, R. D. Hazeltine, and P. J. Morrison, "A generalized reduced fluid model with finite ion-gyroradius effects," *Phys. of Fluids*, vol. 29, pp. 1480–1487, 1986.
[10] Z. Chang and J. D. Callen, "Generalized gyroviscous force and its effect on the momentum balance equation," *Phys. of Fluids B*, vol. 4, pp. 1766–1771, 1992.
[11] J. Wesson, *Tokamaks - third edition*. Oxford University Press, 2004.
[12] INRIA, "Pastix website."
[13] A. Chankin, "this conf.," *Nucl. Energy Mat.*, vol. this conf, 2016.

PACS:52.65.Kj, 52.40.Hf, 52.40.Kh, 52.25.Ya
PSI-21 keywords: Edge modeling, Edge plasma, Drifts
Corresponding author address: CEA, IRFM, 13108 St Paul-Lez-Durance, France.
Corresponding author e-mail: hugo.bufferand@cea.fr
Presenting author: Hugo Bufferand
Presenting author e-mail: hugo.bufferand@cea.fr